J. Fluid Mech. (1990), *vol.* 213, *pp.* 641–655
Printed in Great Britain

A laboratory experiment and numerical simulation of an isolated barotropic eddy in a basin with topographic β

By AKIRA MASUDA[1], KENJI MARUBAYASHI[2] AND MICHIYOSHI ISHIBASHI[2]

[1] Ocean Research Institute, University of Tokyo, Tokyo 164, Japan

[2] Research Institute for Applied Mechanics, Kyushu University, Kasuga 816, Japan

(Received 3 February 1989)

An initial localized eddy was generated in a rotating tank by a source–sink method to study the behaviour of an isolated barotropic eddy on a β-plane. The evolution of the eddy was compared with the laboratory experiments by Firing & Beardsley (1976) and by Takematsu & Kita (1985, 1988), confirming the northwestward (southwestward) translation of a cyclonic (anticyclonic) isolated eddy due to nonlinear effects. Anticyclonic eddies were contrasted with cyclonic eddies in the tank experiment, showing a cyclonic–anticyclonic asymmetry due to the topographic β as a substitute for the planetary β. The fluid experiment was simulated well by numerical simulation based on the quasi-geostrophic vorticity equation. Numerical experiments verified the northwestward (southwestward) translation both for an initially Gaussian and initially Rankine-type isolated cyclonic (anticyclonic) eddy.

1. Introduction

Mesoscale eddies in the ocean have been studied extensively since their discovery about twenty years ago (see Robinson 1983, for a general survey). Nevertheless, many of their behaviours and roles in the ocean circulation still remain unclear. One of the most fundamental problems has been the autonomous behaviour of a barotropic isolated eddy on a β-plane. Many studies have been dedicated to this subject: linear and nonlinear analytical models (Adem 1956; Stern 1975; Flierl 1977, 1987; Nof 1981; Carnevale, Vallis & Purini 1988), numerical simulations (McWilliams & Flierl 1979; Mied & Lindemann 1979; Holloway, Riser & Ramsden 1986), laboratory experiments (Firing & Beardsley 1976), and observtions using moorings, ship surveys and satellite images (see Richardson 1983).

Observational research has reported the seemingly whimsical translation of isolated eddies; they appear to move in any direction (Mizuno & White 1983, for example). Accordingly they are considered to be affected by complicating effects of nearby eddies and currents, geographical and topographic features, and so on. On the other hand, numerical and experimental studies can deal with an isolated eddy independently of such natural complications. They seem to have established a theory that anticyclonic and cyclonic isolated eddies translate in the southwest and northwest directions, respectively, owing to the nonlinearity combined with the β-effect.

Recently, however, it was argued theoretically that isolated eddies do not necessarily follow the accepted theory mentioned above (Nof 1986). Also, a

laboratory experiment by Takematsu & Kita (1985, 1988) reported cyclonic isolated eddies moving southwestward, where the eddies were generated and maintained by local cooling due to a piece of ice floating on the water surface. On this experimental basis, they hypothesized that initially Rankine-type eddies might behave differently from initially Gaussian eddies, to which most of the previous studies have been confined; the former eddies have net vorticity whereas the latter do not. The density stratification used in the experiment of Takematsu & Kita (1985, 1988), however, raises a question as to whether the eddy observed in their experiment is an analogue of an isolated barotropic eddy on a β-plane. Since few laboratory experiments have been performed on this problem, a conclusive laboratory and numerical experiment is needed to clarify this fundamental problem.

Our primary purpose is therefore to examine the northwestward (southwestward) translation of a cyclonic (anticyclonic) isolated eddy by a fluid experiment, which is free of either the restriction of no net vorticity (cf. Firing & Beardsley 1976) or density stratification which complicates the dynamics (cf. Takematsu & Kita 1985, 1988). In this study, an isolated barotropic eddy is produced by a source–sink method satisfying the conditions mentioned above. The second purpose is to test whether the evolution of an eddy in the tank is simulated by a numerical computation based on the quasi-geostrophic vorticity equation. We believe that, in general, the same results obtained from different approaches can afford a reliable solution to a disputable problem. Further, by numerical means, it is possible to compare directly the evolution of an initially Gaussian eddy and an initially Rankine-type eddy. The third purpose lies in contrasting anticyclonic with cyclonic eddies, because previous laboratory experiments have provided flow visualization only of cyclonic ones.

2. Experimental procedures

Parameters are described both in c.g.s. and in non-dimensional units, for the convenience of the description of the tank experiment and the consideration of dynamic balances. Non-dimensional (dimensional) values are often added in parentheses. We non-dimensionalize the variables so that (i) the length of the tank or the basin = 10, (ii) the characteristic $\beta = 1$ and (iii) the characteristic depth of the tank = 1. Then, the horizontal scale (radius) of the initial eddy is about 1 in non-dimensional units in the following experiments.

2.1. *Laboratory experiment*

Figures 1 (*a*) and 1 (*b*) show schematics of the apparatus of the tank experiment in top and side views, respectively. The system is mounted on a turntable. The main tank made of glass is 50.8 cm × 50.8 cm (10 × 10) wide and 30 cm (1.54) deep. Topographic β is introduced by a uniform bottom slope of 1/3. Accordingly, the shallow area corresponds to the northern region in geography. The water in the main tank is 11 cm (0.57) deep in the shallowest portion measured when the turntable is at rest. The tank has a glass lid to reduce surface or friction effects.

The centrifugal force due to the rotation of the tank causes the free surface to assume a parabolic shape. The depth $h(x, y)$ is expressed as

$$h(x,y) = h_r - \frac{y-y_r}{3} - \frac{f_c^2((x-x_r)^2+(y-y_r)^2)}{8g}, \tag{1}$$

where $(x_r, y_r) = (24.0\text{ cm}, 24.1\text{ cm})$ is the rotation axis of the basin, h_r is the depth

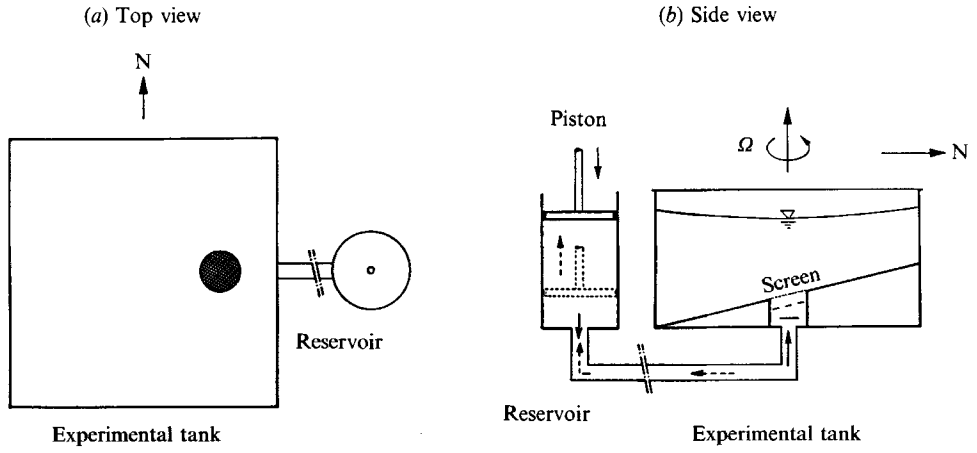

FIGURE 1. Schematic diagram of the tank experiment in (*a*) top view and (*b*) side view. The system rotates at an angular velocity of 19.0 r.p.m. The bottom with slope 1/3 makes the topographic β. An initial localized eddy is generated by a source–sink method; the piston installed at the reservoir tank forces water into or out of the main tank through the net in the hole on the bottom.

there when the system is rotating, f_c the Coriolis parameter and g the acceleration due to gravity. The second term represents the bottom slope. The difference in level between the centre and the marginal area amounts to about 1.3 cm (0.065) because of a rather fast rate of rotation (19.0 r.p.m.). The Coriolis parameter f_c becomes 3.98 s^{-1} (11.5). The characteristic depth around the tank centre (close to the centre of rotation) is estimated to be $h_c = 19.5$ cm (1), from which the topographic β is $f_c(dh/dy)/h_c = 0.0681$ s^{-1} cm^{-1} (1). Thus, the unit horizontal scale, the unit vertical scale and the unit time are 5.08 cm, 19.5 cm and 2.89 s, respectively.

The sloped bottom has a circular hole of radius $r_h = 5.0$ cm (0.98) with the centre at (35.4 cm, 25.4 cm). This hole is covered by a plankton net of fine mesh, through which water can flow, though with much resistance. The screen of the net works like a solid wall except when large forces are exerted so as to force water across it. A pipe connects the hole with a reservoir tank of radius $r_p = 6.25$ cm. It is equipped with a piston with which to force water into or out of the main tank through the screen of the hole. This process generates an initial isolated eddy in the tank.

The vertical motion of the piston is given by

$$z_p = \begin{cases} -A_p \cos\left(\dfrac{2\pi t}{T_p}\right) & \text{for} \quad 0 < t < \frac{1}{2}T_p \\ A_p & \text{for} \quad t > \frac{1}{2}T_p, \end{cases} \tag{2}$$

where z_p is the vertical position of the piston, A_p the amplitude of the displacement of the piston, T_p the period of the sinusoidal motion of the piston, t the time from the start of the piston movement; A_p is positive (negative) for cyclonic (anticyclonic) cases. We set $\frac{1}{2}T_p = 5$ s (1.73) and varied the amplitude $|A_p|$ from 1.5 cm to 3.5 cm.

When the amplitude of the piston displacement $|A_p| = 2.5$ cm, the water column near the hole of the main tank shrinks or stretches by 7.81 cm (0.401). This corresponds to relative vorticity of 1.60 s^{-1} (4.61), which is small compared with the Coriolis parameter $f_c = 3.98$ s^{-1} (11.5) (but of the order of half of f_c). It is large compared with 0.346 s^{-1} (1), the topographic β multiplied by the characteristic scale. In this sense, we may say that the flow is 'quasi-geostrophic' and the eddy is nonlinear.

The decay time due to the bottom Ekman friction is estimated as $h_c/(\frac{1}{2}\nu f_c)^{\frac{1}{2}} =$ 138 s (47.8), where the molecular viscosity $\nu = 0.01$ cm^2 s^{-1} (1.12×10^{-3}). The time constant based on the horizontal viscosity becomes 2580 s (893) for the motion of the unit scale (5.08 cm). Consequently the horizontal viscous effect is small except near the side boundary. Also, the bottom drag can be neglected when we consider the motion within 30 s (10.4) from the onset of the eddy motion.

The flow is visualized by aluminium powder where the light is shed horizontally at the depth of the interior layer. A camera attached to a rotating frame takes photographs from above. We consider that the photograph obtained is representative of the flow at the middle of the exposure time of the film.

2.2. *Numerical experiment*

There are a few difficulties in applying the quasi-geostrophic vorticity equation to the present fluid experiment. First, the aspect ratio of the phenomenon of concern is of order 1; the horizontal scale is even smaller than the vertical scale, if we choose the former at the radius of the initial eddy (5 cm) and the latter at the characteristic depth (19.5 cm). Accordingly the shallow-water assumption does not hold in the present tank experiment. This fact partly reduces the two-dimensionality of motion and partly makes ambiguous the meaning of the (external) radius of deformation. That radius is 34.7 cm (6.83) when it is estimated from $(gh_c)^{\frac{1}{2}}/f_c$, which is valid for shallow water. But the deformation radius becomes 15.8 cm (3.10) when we estimate it from the group velocity of gravity waves with the possible largest wavelength $\sqrt{2} \times 50.8$ cm. The effective deformation radius will be smaller for motions of smaller scales. Since the geostrophic adjustment is not well understood for the case of deep water so far as the authors know, we simply assume the latter value of 15.8 cm for the deformation radius; an infinite and other values of deformation radius were tested, but qualitatively similar results were confirmed.

The second difficulty is concerned with the expected large relative vorticity (about half of f_c, see the preceding section) and the third with the large bottom slope of 1/3. These are unfavourable for the quasi-geostrophic approximation. If more precise simulation is intended for the present laboratory experiments, we should rely on the primitive equations which can describe the adjustment process by external inertio-gravity waves with aspect ratio of order 1. Here, however, we restrict ourselves to the quasi-geostrophic regime with suitable modifications, partly for computational economy and partly to simplify the dynamics. It is expected that qualitative features of the tank experiment will be reproduced by the quasi-geostrophic equation as well, since the fundamental dynamics is due to eddies rather than gravity waves.

In a preliminary report (Masuda, Marubayashi & Ishibashi 1987*b*), we solved an initial-value problem for the non-dimensional quasi-geostrophic vorticity equation on a β-plane with an initially Gaussian eddy. Here we introduce the topographic β explicitly by the depth distribution of (1), in order to represent better the topographic β of the tank experiments. We remark that the results are qualitatively the same as in the preliminary study on a plane of uniform β, except for the north–south asymmetry described in the next section.

The basic equation we use for the numerical experiments is

$$\frac{\partial}{\partial t}\{\nabla^2\psi - \nu^2\psi\} + J(\psi, \nabla^2\psi) + hJ\left(\psi, \frac{f_c}{h}\right) = -\left(\frac{\nu f_c}{2h^2}\right)^{\frac{1}{2}}\nabla^2\psi + \nu\nabla^4\psi + V_i, \tag{3}$$

where ψ is the 'quasi-geostrophic' stream function, t the time, (x, y) the (eastward, northward) coordinates, $\gamma^2 = 0.103$ (4.01×10^{-3} cm^{-2}) the square inverse of the

deformation radius, ∇^2 the Laplacian operator, J the Jacobian operator and V_i the vorticity input, defined later (Pedlosky 1987). The third term expresses the topographic β, where $h(x, y)$ is given by (1). The constant factor h_c might be preferred to $h(x, y)$ in this term or in the bottom stress term for consistency of the geostrophic approximation. However, we adopted the present form since it gave a (slightly) better agreement with the laboratory experiment and since it partly takes into consideration the large bottom slope, which cannot be described precisely by the geostrophic approximation, as mentioned before. A finite-difference method is used for time integration. The computational area is 10×10 square, the grid intervals are $\Delta x = \Delta y = 0.2$ (1.16 cm), and the time step $\Delta t = 3.46 \times 10^{-2}$ (0.1 s). We include small viscous terms, but presumably they hardly affect the overall behaviour of the eddy. For computational simplicity we adopt the slip condition at the side boundary, since the non-slip condition requires much finer grids for the resolution of the viscous boundary layer.

Three kinds of numerical experiments are presented here: (i) the initial-value problem of a Gaussian eddy, (ii) the initial-value problem of a Rankine-type eddy and (iii) the response problem to the vorticity input. The initially Gaussian eddy is described by

$$\psi(x, y) = P \exp\left\{-\frac{(x-x_h)^2+(y-y_h)^2}{r_c^2}\right\}, \tag{4}$$

where $(x_h, y_h) = (35.4\text{ cm}, 25.4\text{ cm})$ denotes the location of the centre of the hole, r_c the characteristic radius, and P the amplitude of the initial Gaussian stream function. We evaluate the amplitude P so that the maximum vorticity is twice the expected vorticity input averaged over the hole; $P = A_p f_c (r_p r_c / r_h)^2 / h_c$.

For the Rankine-type eddy, the initial stream function is the solution of the equation

$$\nabla^2\psi - \gamma^2\psi = \begin{cases} Q\left(\dfrac{r_p}{r_h}\right)^2 2\left(1-\dfrac{r^2}{r_c^2}\right) & \text{for } r_c < r \\ 0 & \text{otherwise,} \end{cases} \tag{5}$$

where $r^2 = (x-x_h)^2 + (y-y_h)^2$ and Q denotes the amplitude of the potential vorticity; Q is evaluated as $2A_p(r_p/r_h)^2 (f_c/h_c)$.

In the response problem, we consider the vorticity input to be given by the vertical velocity at the bottom of the hole, which is approximated here as

$$w(x, y, t) = \begin{cases} \left(\dfrac{r_p}{r_h}\right)^2 \dfrac{2\pi}{T_p} A_p \sin\left(\dfrac{2\pi}{T_p} t\right) 2\left(1-\dfrac{r^2}{r_h^2}\right) & \text{for} \\ & 0 < r < r_h \text{ and } 0 < t < \tfrac{1}{2}T_p \\ 0 & \text{otherwise.} \end{cases} \tag{6}$$

The vorticity input then becomes

$$V_i(x, y, t) = \frac{f_c}{h(x, y)} w(x, y, t). \tag{7}$$

In the above rough arguments, the (possibly) maximum amplitudes are estimated. We do not know precisely, however, which inflow or outflow rate through the net is actually used for the generation of the isolated eddy. Also we do not know which functional form of forcing in the hole is adequate or which characteristic radii are appropriate in substituting the initial-value problem for the response problem. We therefore consider, irrespective of the intensity or the sign of the eddy, (i) an

'efficiency' coefficient $c_e = 0.7$, (ii) a parabolic form of forcing (see (5) and (6)) and (iii) $r_c = 1.2r_h$; these assumptions provided reasonable flows in agreement with the tank experiment. We tested a larger c_e of about 1, a uniform forcing or a smaller r_c, but obtained similar flows. It is worthwhile to note (i) that a larger c_e and uniform forcing give a similar flow to a smaller c_e and a parabolic distribution of forcing, and (ii) that the cyclonic (anticyclonic) case is simulated better by a larger (smaller) c_e and a parabolic (uniform) form of forcing on the hole. These may be ascribed to the source–sink method used for the generation of the eddy.

3. Results

There are various experimental constraints which reduce the validity of the quasi-geostrophic approximation, as mentioned before. We should therefore ignore detailed discrepancies and be satisfied with qualitative agreement of the flow pattern between the laboratory and numerical experiments. We contrast an anticyclonic with a cyclonic eddy, since no visualization is available for the former and it shows an evolution different from that of the cyclonic eddy in a basin with topographic β.

Figures 2 and 3 are presented to show the almost linear eddy field at $t = 13.5$ s and 21.5 s, respectively. The photographs were obtained for a cyclonic eddy of small (but finite) amplitude $A_p = 1.5$ cm with a long exposure time, $T_e = 3$ s, required to visualize the slow motion of this case. Numerical linear response was calculated for the anticyclonic input. Considering the time needed for geostrophic adjustment, we shifted the time of numerical simulation by an amount of 1.5 s. Solid and dashed lines respectively represent positive and negative contours of ψ. The contour interval is always taken at 0.1 times the maximum absolute value of the stream function at the corresponding moment; it is arbitrary for the linear case. The flow has a north–south asymmetry even for the linear computation. In particular, the secondary eddy to the northeast of the main eddy propagates faster than that to the southeast. This feature is due to the larger topographic β $(= f_c(\mathrm{d}h/\mathrm{d}y)/h)$ in the northern (shallow) area of the basin. In the fluid experiment, the cyclonic eddy moves slightly in the northwestward direction, indicating a finite-amplitude effect. We see that the linear simulation is in good agreement with the observed evolution of the eddy of small amplitude in the tank.

Figures 4–7 (*a*) show the typical nonlinear evolution of a cyclonic eddy in a rotating tank visualized by aluminium powder at four instances for a single experimental run; $T_e = 1$ s. The amplitude of the piston ($A_p = 3.5$ cm) is the largest in the present laboratory experiment. Figures 4–7 (*c*) show the same as figures 4–7 (*a*) but for an anticyclonic eddy ($A_p = -3.5$ cm). Numerical simulations are shown in figures 4–7 (*b*) and (*d*), corresponding to (*a*) and (*c*), respectively. Taking into account the problems associated with the quasi-geostrophic approximation and the difficult control of the generation of the initial eddy by the source–sink method, we may say that the experimental and numerical experiments have nearly the same conditions.

The eddy is generated at $t = 4.5$ s (figure 4). The flow still preserves the north–south symmetry. Noticeable motion is observed in most of the basin, but the numerical results give a wider spread of motion presumably due to the quasi-geostrophic formulation; probably we should take a smaller deformation radius or consider the more precise adjustment process. In the fluid experiment, the anticyclonic case has an irregular motion near the eddy centre, since the inflow up through the screen induces turbulence; this probably accounts for why a smaller c_e and the uniform forcing on the hole would be preferred for the anticyclonic case.

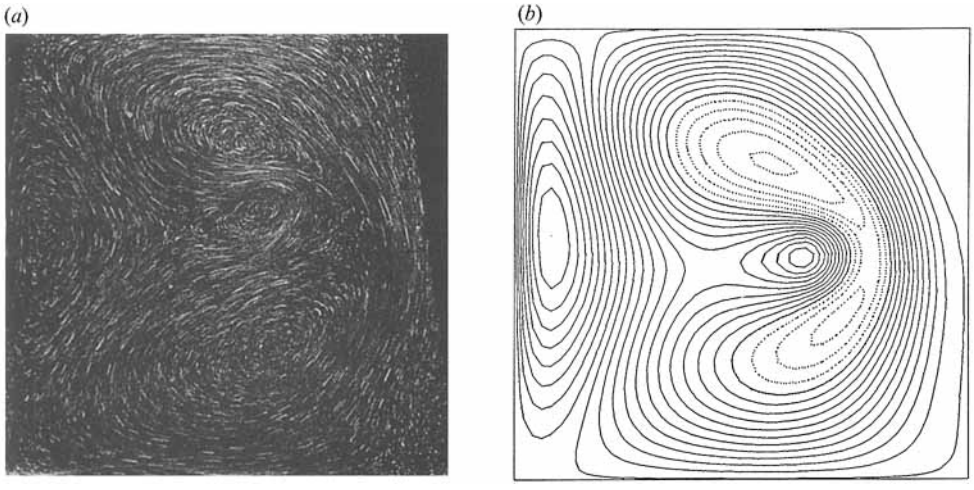

FIGURE 2. Almost linear response of the eddy field at $t = 13.5$ s from the start of the piston of the reservoir tank in (*a*) the laboratory and (*b*) the numerical experiment. In the laboratory experiment the amplitude of the piston $A_p = 1.5$ cm (cyclonic), while the stream function was computed by a numerical simulation of the response kind (see text). The time for (*b*) is delayed by 1.5 s as the time necessary for the geostrophic adjustment. The contour interval is arbitrary for this linear case. Solid and dashed lines represent positive and negative contours, respectively.

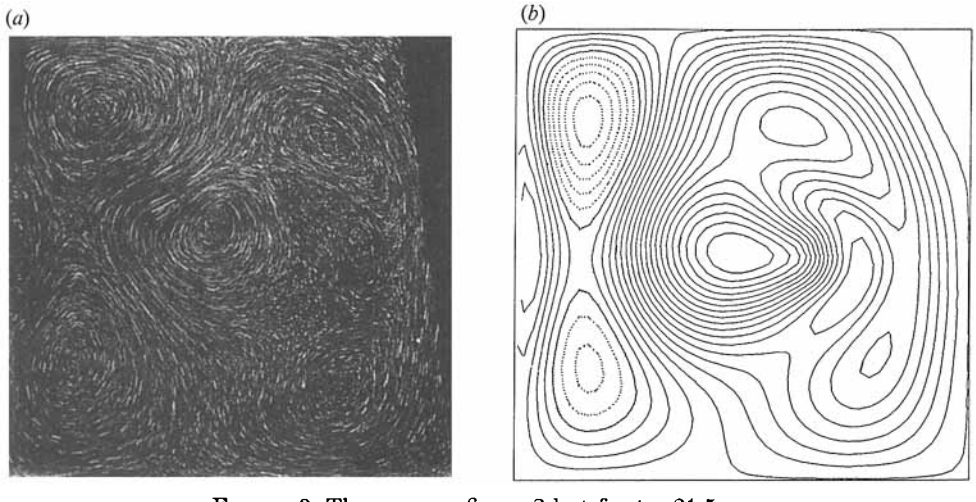

FIGURE 3. The same as figure 2 but for $t = 21.5$ s.

Later, at $t = 12.5$ s in figures 5(*a*) and 5(*b*), the cyclonic main eddy moves northwestward and secondary anticyclonic eddies appear to the northeast and to the southeast of the main cyclonic eddy. The main eddy takes a more circular form than in the linear case in figure 2. Strong nonlinearity enhances the secondary eddy in the southeastern area more than in the northeastern. We do not observe many alternating eddies elongated meridionally to the east of the main eddy as anticipated from previous theoretical and numerical studies of an isolated eddy in a wide basin. We must note that the present experiment deals with an eddy of larger scale than that in the previous experiments. Accordingly the side boundary has stronger effects

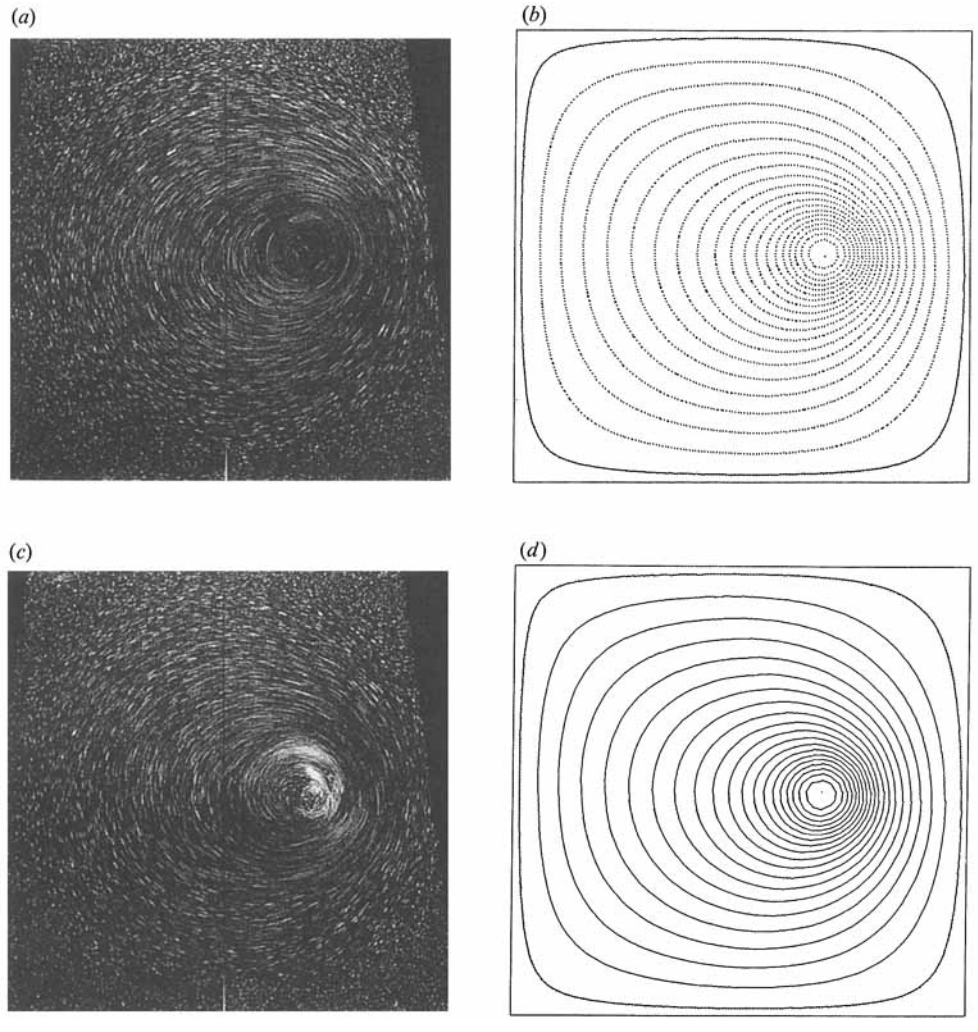

FIGURE 4. Eddy field at $t = 4.5$ s for strongly nonlinear case of $|A_p| = 3.5$ cm: (*a*) cyclonic eddy in the tank experiment, (*b*) cyclonic eddy in the numerical simulation, (*c*) anticyclonic eddy in the tank and (*d*) anticyclonic eddy in the numerical simulation. The contour interval is 1.36 $cm^2\ s^{-1}$ for (*b*) and 1.35 $cm^2\ s^{-1}$ for (*d*).

on the eddy motion and thereby Rossby normal modes of basin-wide scale will be important.

Near the western boundary, long Rossby waves are reflected as short Rossby waves, causing a secondary cyclonic eddy. In the numerical experiment, it moves southward like the boundary Batchelor-modon eddy (Yasuda, Okuda & Mizuno 1986; Masuda, Marubayashi & Ishibashi 1987*a*; Masuda 1988), whereas such a translation is only just observed in the fluid experiment. This is mainly because the quasi-geostrophic formulation transfers more energy westward than the real motion (compare the fluid experiment with the numerical experiment at $t = 4.5$ s). Another reason is the slip boundary condition of the numerical simulation; the non-slip condition adequate for the fluid experiment would resist this translation of the eddy. The anticyclonic eddy of figures 5(*c*) and 5(*d*) shows similar behaviour, if we interchange 'north' and 'south'. A notable quantitative difference between the tank

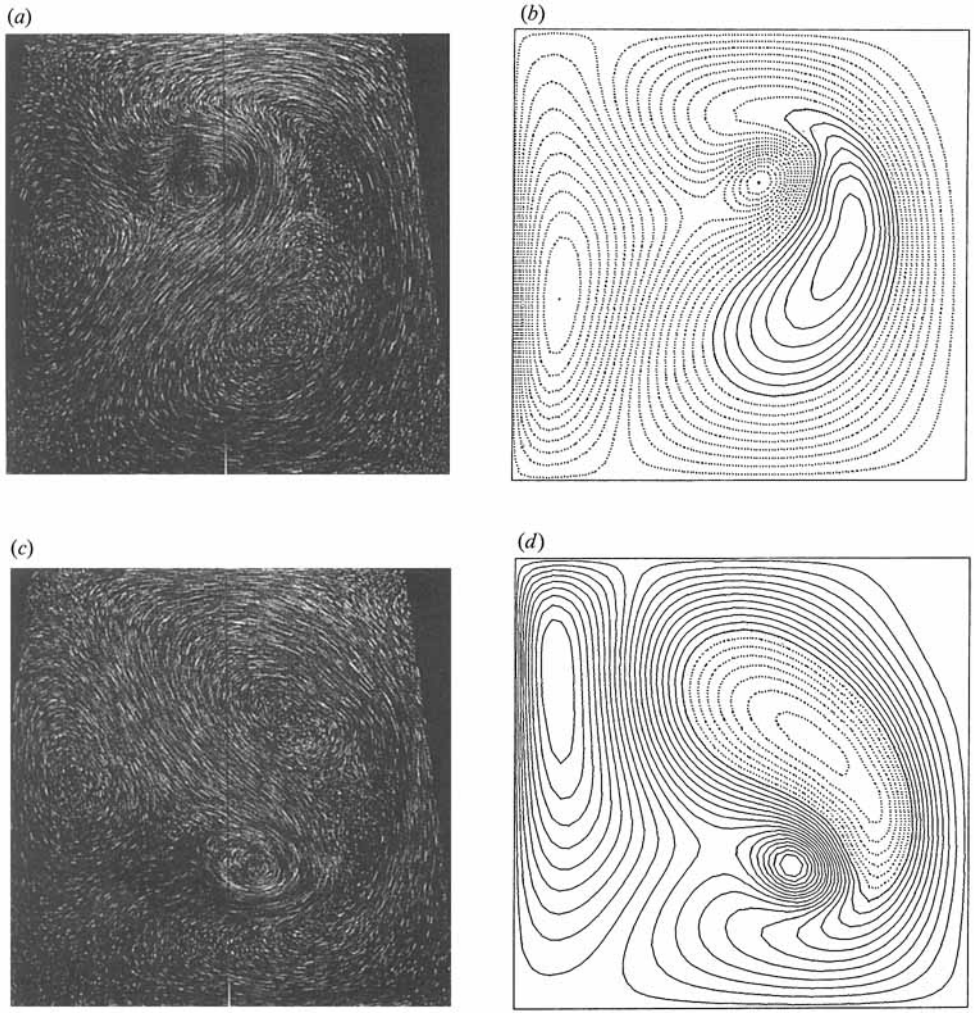

FIGURE 5. The same as figure 2 but for $t = 12.5$ s: contour interval is 1.07 cm^2 s^{-1} for (*b*) and 0.991 cm^2 s^{-1} for (*d*).

experiment and the numerical experiment is the faster westward translation of the main eddy in the former.

Figure 6 shows the flow a little later at $t = 16.5$ s. The elongated eddy near the western boundary seems to disappear in the fluid experiment, but it reaches the southwest or the northwest corner in the numerical experiment. The main cyclonic (anticyclonic) eddy barely translates farther northwest (southwest) in this period (see figure 10). At this time, the main eddy is passed by the secondary eddies which were located to the east but now to the west of the main eddy, since these secondary eddies propagate rapidly owing to their large scale. To the east of the secondary eddies, tertiary eddies of opposite signs are generated, propagating westward. The flow at $t = 26.5$ s is shown in figure 7. Eddies of different scales appear in the eastern basin. The main eddy enlarges its area and approaches the western boundary at an accelerated pace. The secondary eddies which have preceded the main eddy are reflected by the western boundary and they will disappear. We observe clear north–south (cyclonic–anticyclonic) asymmetry in this figure.

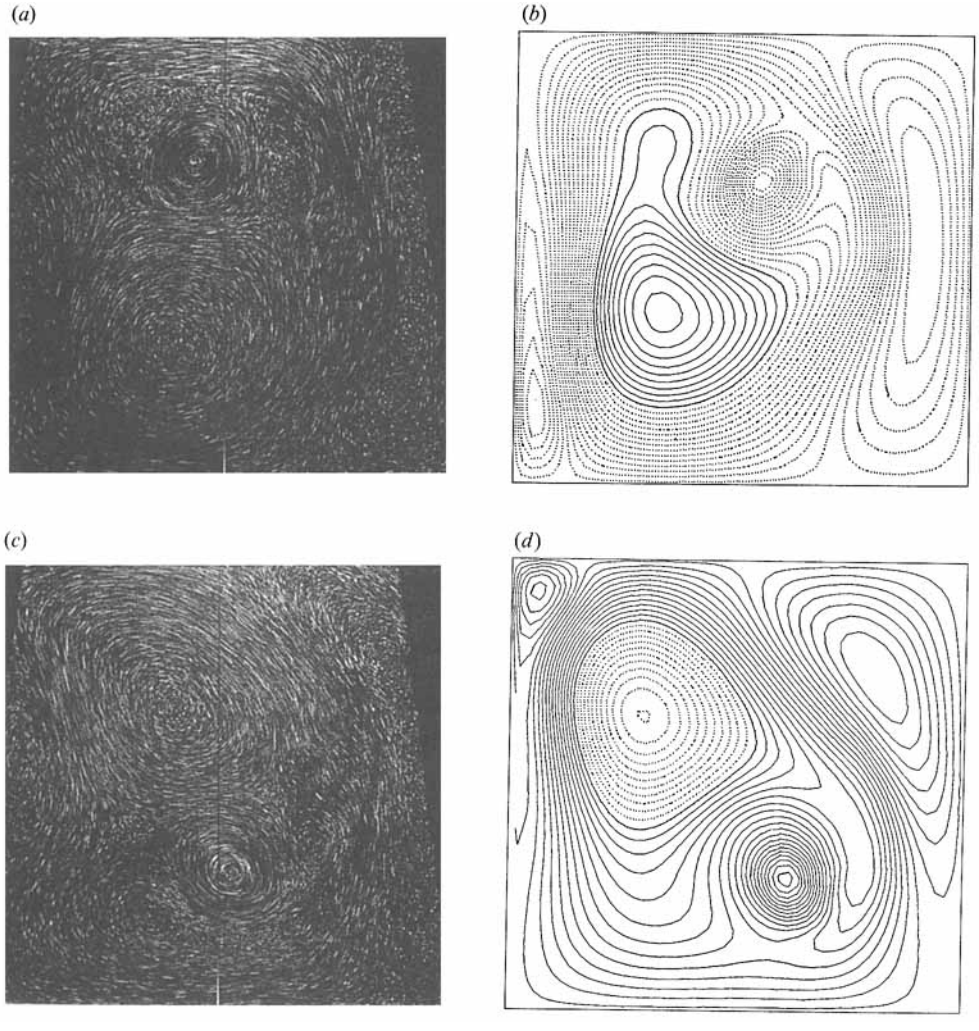

FIGURE 6. The same as figure 2 but for $t = 16.5$ s: contour interval is 0.813 cm^2 s^{-1} for (*b*) and 0.895 cm^2 s^{-1} for (*d*).

Next, let us examine the evolution of the initial isolated eddy. Figures 8 and 9 show the simulated eddy field at $t = 9$ and 13 s, respectively, for (*a*) a Rankine-type cyclonic and (*b*) a Gaussian cyclonic case, where the initial distribution is described in §2.2. The amplitude is the same as in figures 4–7. If we delay by 3.5 s, the time necessary for the initial generation and the geostrophic adjustment, figures 8 and 9 correspond to figures 3 and 4. The flow of initially Rankine-type eddies is almost the same as the simulation of the response type; in particular, the secondary eddy formed near the western boundary translates like the boundary Batchelor-modon type eddy. For the Gaussian distribution, intense motion is concentrated near the main eddy and the scale of the eddy is relatively small. Consequently the secondary eddies propagate westward more slowly for the Gaussian eddy. Anticyclonic cases were simulated as well for the same kind of initial eddies, showing their southwestward translation.

Finally, figure 10 plots the trajectories of the eddy centre for $A_p = \pm 2.5$ and

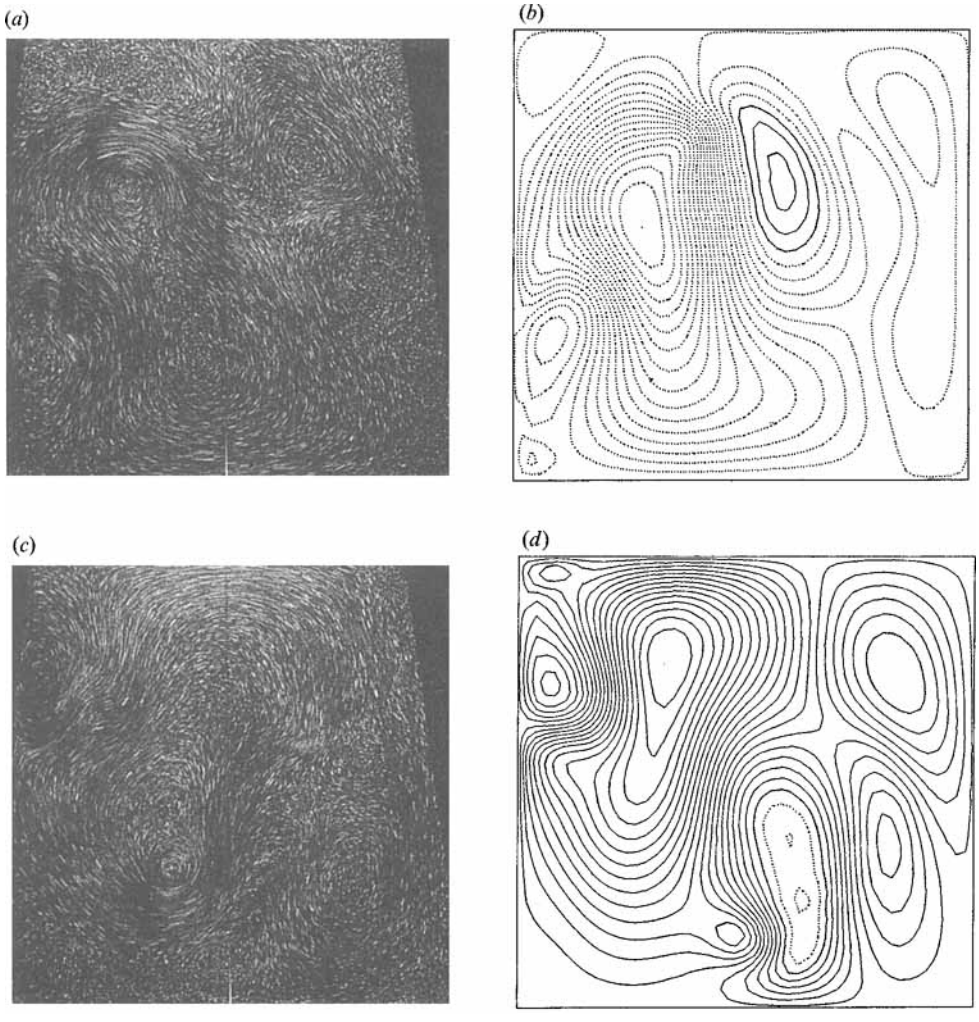

FIGURE 7. The same as figure 2 but for $t = 26.5$ s: contour interval is 1.17 cm^2 s^{-1} for (*b*) and 1.01 cm^2 s^{-1} for (*d*).

± 3.5 cm, where the tracing was made from the photographs of the flow taken at every 2 s. The hole at the bottom is drawn as a circle in the figure. We observe that the cyclonic eddy moves westward faster than the anticyclonic eddy, but the northward translation of the former eddy is small compared with the southward translation of the latter eddy. The larger the nonlinearity or $|A_p|$, the larger is the northward (southward) translation. During the time from about 12 s to about 20 s, a significant motion of the eddy centre is found. The eddy seems stagnant in westward translation; it moves to the north (south) and returns back a little to the south (north) for the cyclonic (anticyclonic) case. Then it begins to translate or propagate westward with a large speed.

The observed trajectories of the eddy centre may be interpreted as follows for the cyclonic case (see the sequences of figures 4–7 *a* and *c*). As the secondary eddies grow to the east of the main eddy, they accelerate the northward translation of the main eddy. By virtue of the stronger topographic β mentioned in the linear case, the

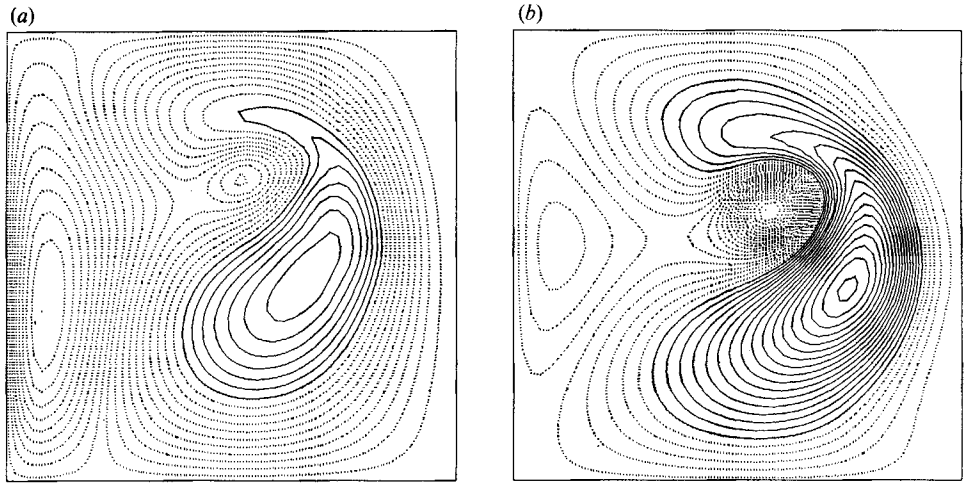

FIGURE 8. Simulated eddy field corresponding to $t = 12.5$ s for the initially cyclonic (*a*) Rankine-type and (*b*) Gaussian isolated eddy: contour interval is (*a*) 1.07 cm^2 s^{-1} and (*b*) 0.685 cm^2 s^{-1}. The time is delayed by 3.5 s.

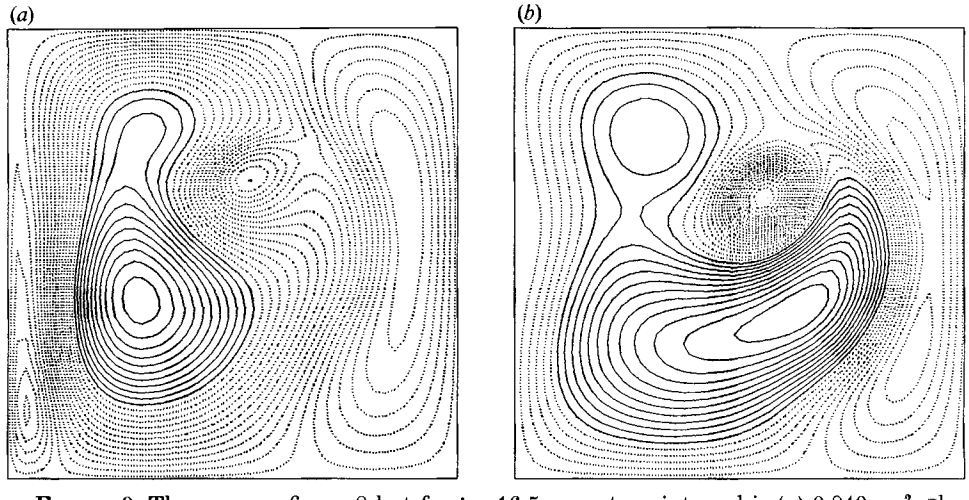

FIGURE 9. The same as figure 8 but for $t = 16.5$ s: contour interval is (*a*) 0.840 cm^2 s^{-1} and (*b*) 0.930 cm^2 s^{-1}.

northern area increases the westward propagation, but decelerates the northward translation since nonlinearity is measured relative to the β-effect. Of course, large amplitude increases the northward translation of the main eddy due to nonlinearity. Since the secondary eddies propagate faster than the main eddy by virtue of their large scale, they soon run parallel to the main eddy. In this period, they induce a flow that pushes the main eddy back eastward (this is not inherent to the nonlinear case only, but also occurs for the linear response computed numerically). They eventually outrun the main eddy, causing a southward backing motion of the main cyclonic eddy. After they propagate far westward, the main eddy enlarges its scale and proceeds westward rapidly as Rossby waves.

Though slightly underestimating the westward translation velocity of the main eddy, the numerical simulation reproduced the characteristic trajectory of the main

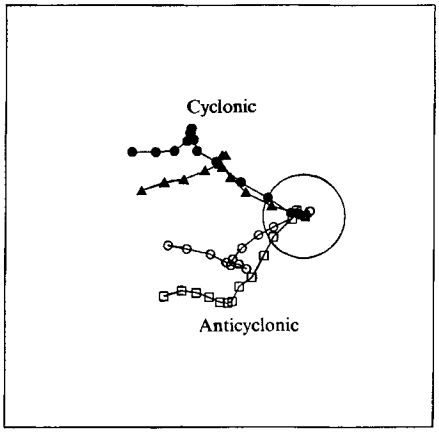

FIGURE 10. Trajectories of the eddy centre, where the tracing was made from the visualized flow of the tank experiment every 2 s: ●, $A_p = 3.5$ cm; ▲, $A_p = 2.5$ cm; ○, $A_p = -2.5$ cm; □, $A_p = -3.5$ cm. The solid symbols correspond to cyclonic eddies and the open ones to anticyclonic eddies.

eddy: (i) the northwestward (southwestward) translation direction of a cyclonic (anticyclonic) eddy, (ii) the positive dependence of the meridional translation velocity on nonlinearity, (iii) faster (slower) westward but slower (faster) northward (southward) translation of a cyclonic (anticyclonic) eddy, and (iv) a peculiar motion around $t = 12$ s to $t = 20$ s. Only in the simulation of a Gaussian eddy, does the cyclonic (anticyclonic) eddy tend to move northward (southward) in a monotonic manner; this fact suggests the importance of large-scale (basin-wide) eddies for the meridional pulling back of the main eddy.

4. Conclusions and discussion

To study the autonomous behaviour of isolated eddies on a β-plane, a laboratory and numerical experiment was carried out. In the laboratory experiment, a source–sink method was used to generate an initial localized eddy. Thus, the system is free of density stratification in contrast to that of Takematsu & Kita (1985, 1988) and the initial eddy has net vorticity in contrast to the Gaussian eddy studied by Firing & Beardsley (1976).

The numerical simulation was based on the quasi-geostrophic vorticity equation with some modifications. A few difficulties were unavoidable in approximating the present tank experiment by the quasi-geostrophic regime, especially with regard to the aspect ratio and the adjustment process. If an improved simulation is intended, we should rely on a primitive equation approach. Also, it was difficult to control sufficiently well the generation of the initial eddy by the source–sink method.

Nevertheless the quasi-geostrophic vorticity equation yields a good computational analogue of the laboratory experiment; it was confirmed that the numerical experiment simulates the fluid experiment remarkably well, not only the flow pattern but also the trajectory of the main eddy. The qualitative behaviour of the eddy is insensitive to the initial conditions and the radius of deformation. In particular, the numerical computation based on the quasi-geostrophic vorticity equation shows that a cyclonic (anticyclonic) barotropic isolated eddy translates northwestward (southwestward), irrespective of whether it is a Gaussian eddy or a

Rankine-type eddy, i.e. irrespective of whether the isolated eddy has net vorticity or not. In other words, the overall behaviour of the isolated eddy is not sensitive to the initial net vorticity of the eddy.

Thus, we can conclude that a cyclonic eddy on a β-plane certainly translates northwestward in accordance with most of the previous findings (Firing & Beardsley 1976). At the same time, the present results suggest that the cyclonic eddies translating southwestward as observed in the laboratory experiments of Takematsu & Kita (1985, 1988) are governed by more subtle dynamics related with density stratification.

Carrying out the experiment for both the cyclonic and anticyclonic case, we confirmed the north–south asymmetry due to nonlinear effects. When the planetary β is substituted by the topographic β, however, another north–south asymmetry is introduced. Since the topographic β is stronger in the northern area (note the opposite situation on the Earth), Rossby waves at higher latitudes propagate westward more rapidly than those at low latitudes. Consequently nonlinear effects are exaggerated in the southern area. These features were confirmed both in the tank experiment and in the numerical experiment.

The translation of the eddy has often been discussed in relation to the eddy transport of various physical, chemical and biological quantities. As an example, let us attempt a simple argument on the meridional transport of (potential) vorticity by isolated eddies. The present results imply that the northward vorticity flux is positive irrespective of the sign of the isolated eddy; for the cyclonic (anticyclonic) eddy, the vorticity is positive (negative) and the translation is northward (southward). If the distribution of isolated eddies has a maximum at a latitude, its northern area receives positive vorticity input, while the southern area receives negative input. Then the maximum latitude will be accelerated eastward and both sides will accept the westward momentum. This consequence might have a close relation with eddy-driven circulation (both of the surface and of the bottom layer) or the recirculation of the Kuroshio or the Gulf Stream (Holland 1978; Holland & Rhines 1980). Of course, the present crude argument should be modified by vorticity transport due to eddies of non-isolated forms and other effects such as density stratification, nearby currents or eddies.

The authors would like to appreciate Ms M. Hojo for typing. This work was partly supported by a Priority area program, Dynamics of the deep ocean circulation, defrayed by the Ministry of Education, Science and Culture, Japan.

REFERENCES

Adem, J. 1956 A series solution of barotropic equation and its application in the study of atmospheric vortices. *Tellus* **8**, 364–372.

Carnevale, G. F., Vallis, G. K. & Purini, R. 1988 Propagation of barotropic modons over topography. *Geophys. Astrophys. Fluid Dyn.* **41**, 45–101.

Firing, E. & Beardsley, R. C. 1976 The behavior of a barotropic eddy on a β-plane. *J. Phys. Oceanogr.* **6**, 57–65.

Flierl, G. R. 1977 The application of linear quasi-geostrophic dynamics to Gulf Stream Rings. *J. Phys. Oceanogr.* **7**, 365–379.

Flierl, G. R. 1987 Isolated eddy models in geophysics. *Ann. Rev. Fluid Mech.* **19**, 493–530.

Holland, W. R. 1978 The role of mesoscale eddies in the general circulation of the ocean-numerical experiments using a wind driven quasi-geostrophic model. *J. Phys. Oceanogr.* **8**, 363–392.

HOLLAND, W. R. & RHINES, P. B. 1980 An example of eddy-induced ocean circulation. *J. Phys. Oceanogr.* **10**, 1010–1031.

HOLLOWAY, G., RISER, D. C. & RAMSDEN, D. 1986 Tracer anomaly evolution in the flow field of an isolated eddy. *Dyn. Atmos. Oceans* **10**, 165–184.

MASUDA, A. 1988 A skewed eddy of Batchelor-modon type. *J. Oceanogr. Soc. Japan* **44**, 189–199.

MASUDA, A., MARUBAYASHI, K. & ISHIBASHI, M. 1987*a* Batchelor-modon type eddies and isolated eddies near the coast of an *f*-plane. *J. Oceanogr. Soc. Japan* **43**, 383–394.

MASUDA, A., MARUBAYASHI, K. & ISHIBASHI, M. 1987*b* A laboratory and numerical experiment on the behavior of an isolated barotropic eddy on a *β*-plane. *Rep. Res. Inst. Appl. Mech., Kyushu University*, vol. 65, pp. 67–78 (in Japanese).

MCWILLIAMS, J. C. & FLIERL, G. R. 1979 On the evolution of isolated nonlinear vortices. *J. Phys. Oceanogr.* **9**, 1155–1182.

MIED, R. P. & LINDEMANN, G. R. 1979 The propagation and evolution of cyclonic Gulf Stream rings. *J. Phys. Oceanogr.* **9**, 1183–1206.

MIZUNO, K. & WHITE, B. 1983 Annual and interannual variability in the Kuroshio Current System. *J. Phys. Oceanogr.* **13**, 154–159.

NOF, D. 1981 On the *β*-induced movement of isolated barotropic eddies. *J. Phys. Oceanogr.* **11**, 1162–1172.

NOF, D. 1986 Movements and interactions of isolated eddies. *Summer Study Program in Geophysical Fluid Dynamics, Woods Hole Oceanographic Institution*, pp. 120–122.

PEDLOSKY, J. 1987 *Geophysical Fluid Dynamics*, 2nd edn. Springer. 710 pp.

RICHARDSON, R. L. 1983 Gulf Stream rings. In *Eddies in Marine Science* (ed. A. R. Robinson), pp. 19–45. Springer.

ROBINSON, A. R. (ed.) 1983 *Eddies in Marine Science*. Springer.

STERN, M. E. 1975 Minimal properties of planetary eddies. *J. Mar. Res.* **33**, 1–13.

TAKEMATSU, M. & KITA, T. 1985 The behavior of an isolated free eddy in a rotating fluid (a laboratory experiment). *Rep. Res. Inst. Appl. Mech., Kyushu University*, vol. 33, pp. 1–12.

TAKEMATSU, M. & KITA, T. 1988 The behavior of an isolated free eddies in a rotating fluid: Laboratory experiment. *Fluid Dyn. Res.* **3**, 400–406.

YASUDA, I., OKUDA, K. & MIZUNO, K. 1986 Numerical study on the vortices near boundaries – considerations on warm core rings in the vicinity of east coast of Japan. *Bull. Tohoku Regional Fisheries Res. Lab.* **48**, 67–86.